Time-Modulated Antenna Array for Real-Time Adaptation in Wideband Wireless Systems—Part II: Adaptation Study

Grzegorz Bogdan, *Member, IEEE,* Konrad Godziszewski, *Member, IEEE,* and Yevhen Yashchyshyn, *Senior Member, IEEE*

***Abstract*—In this paper, an adaptive antenna system (AAS) based on a time-modulated antenna array (TMAA) and population-based metaheuristic algorithm is presented. The algorithms is driven by the signal-to-noise ratio measurements and provides real-time adaptation of the antenna pattern. This paper also addresses the issue of multi-band reception with a TMAA, demonstrating that the sidebands generated from frequency-diverse signals can overlap and interfere. The effectiveness of the AAS as part of a wireless communication system is presented in three different experimental scenarios that consider gradually or rapidly changing conditions as well as the interference caused by the reception of two signals with different carrier frequencies.**

***Index Terms*—adaptive antennas, adaptive systems, beam-steering, communication systems, digital communication, interference suppression, microwave communication, optimization methods, radio-frequency (RF) switch, time-modulated antenna arrays.**

I. Introduction

ADAPTIVE antenna systems (AASs) combine controllable hardware and an optimization algorithm to deliver a maximum fidelity signal via automatic separation of the desired signal from interfering signals by controlling the shape of the antenna pattern. Traditionally, deterministic methods have been used for adaptive array processing, such as the least mean square algorithm [1], constant modulus algorithm [2], and conjugate gradient method [3]. Nowadays, however, biological beamforming algorithms have been widely implemented in various electromagnetic applications [4]. One of the most popular is the genetic algorithm (GA), which has been used to control adaptive systems by adjusting some of the least significant bits of digitally controlled phase shifters [5], [6] as well as to calculate optimal values for the reactance loading of parasitic elements [7]. Previously, algorithms based on a binary-coded GA were applied in many adaptive antennas [8]–[10]; however, they did not consider constantly changing conditions or the need to readapt to new environments once the population converges, which is crucial in practice. This problem has since been solved using diploidy and dominance [11] or cooperative algorithms [12]. Other types of biologically inspired algorithms used for the synthesis of antenna patterns include the differential evolution [13]–[15], particle swarm optimization [16], invasive weed optimization [17], and the artificial bee colony [18].

Grzegorz Bogdan, Konrad Godziszewski and Yevhen Yashchyshyn are with the Institute of Radioelectronics and Multimedia Technology, Warsaw University of Technology, Warsaw, 00-665 Poland e-mail: {g.bogdan, k.godziszewski, y.yashchyshyn}@ire.pw.edu.pl

The conventional types of adaptive antenna are the phased antenna array [19], antenna with reconfigurable aperture [20], and antenna array with digital beamforming [21]. Despite extensive research and development, AASs are not yet suitable for inexpensive wireless devices due to their complexity, cost, and energy consumption. Time-modulated antenna arrays (TMAAs) are an alternative solution that offers a series of key advantages compared with conventional phased arrays or digital beamforming systems. A TMAA is an electromagnetic system whose radiated power pattern is controlled by the application of periodic pulses to the individual elements [22]. Its known applications include beamforming [23], wireless communication [24], [25], and reconfigurable wireless power transmission [26]. Although the TMAA is a potential candidate for low-cost AASs, it also possesses limitations and drawbacks. For instance, when used in transmit mode, its inherently generated sidebands may interfere with other systems operating in adjacent frequency bands. However, this problem could be solved with special TMAA architectures that produce only one sideband or significantly attenuate the power of undesired sidebands [27]–[29]. Another solution could be to use the TMAA as a receiving antenna, although this may also be problematic since a TMAA is usually capable of accepting signals for a wider bandwidth than required. Therefore, for cases of wireless networks with dense spectrum allocation, unwanted signals from adjacent channels may be received and time-modulated together with the desired signal. Consequently, the sidebands generated from frequency-diverse signals may overlap and interfere in the receiver. This peculiarity, which does not occur in conventional antenna systems, may be a significant disadvantage limiting the applicability of TMAAs in practical wireless networks.

This paper is organized as follows: In Section II, the mathematical model of a receiving TMAA is given and the unwanted interference of sidebands is discussed. A potential solution to this issue, i.e., an adaptive algorithm to maximize the signal-to-noise ratio (SNR), is presented in Section III. An experimental verification of the TMAA controlled by the adaptive algorithm is presented in Section IV. Finally, the conclusions are given in Section V.

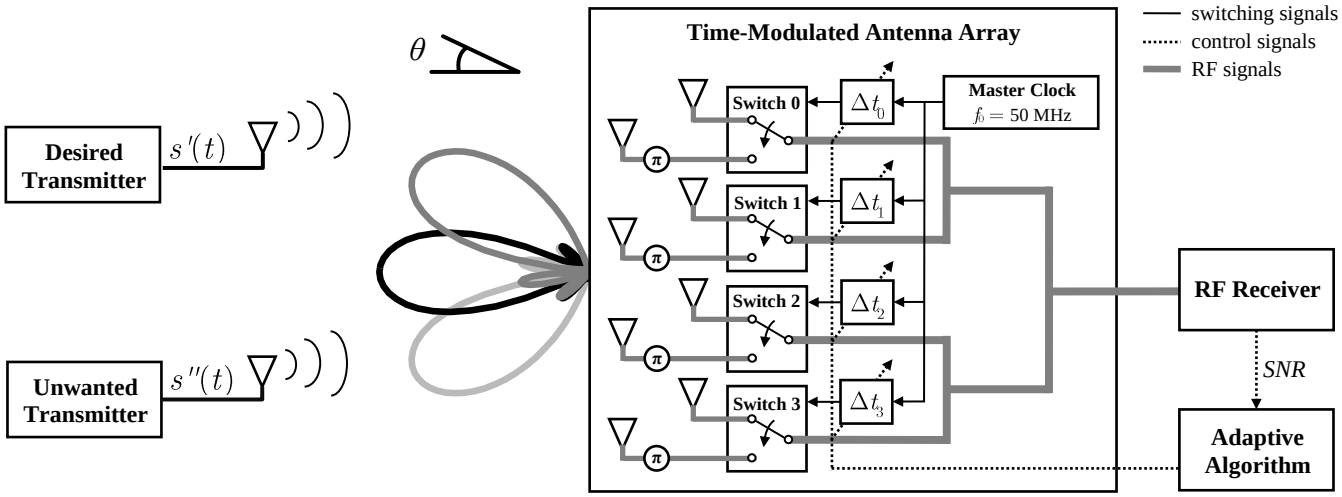

Fig. 1. General concept of a receiving AAS based on a TMAA.

II. TMAA

A. Mathematical Formulation of the Array Factor

The array factor of the receiving TMAA can be formulated as:

$$AF(\theta,t) = e^{j2\pi f_c t}\sum_{n=0}^{N-1} S_n m_n(t) e^{j\beta n d\sin\theta} \tag{1}$$

where, the term $e^{j2\pi f_c t}$ expresses periodic oscillations, $n \in \{0,\ldots,N-1\}$ is the index of an element in the array, S_n is the complex excitation of the n-th antenna element induced by an impinging signal $s(t)$, f_c is the carrier frequency of $s(t)$, $m_n(t)$ is the modulating function applied to the n-th antenna element in the array, $\beta = 2\pi f_c/c$ is the wavenumber, c is the speed of the electromagnetic wave, d is the distance between the uniformly-spaced antenna elements in the array, and θ is the angle with respect to the normal to the antenna array main axis. By virtue of the Fourier series expansion, each periodic function $m_n(t)$ can be expressed as a sum of complex coefficients $M_n[k]$:

$$m_n(t) = \sum_{k=-\infty}^{+\infty} M_n[k] e^{j2\pi f_0 k t} \tag{2}$$

$$M_n[k] = \frac{1}{T_0}\int_{\frac{-T_0}{2}}^{\frac{T_0}{2}} m_n(t) e^{-j2\pi f_0 k t} dt \tag{3}$$

where k represents the index of the complex Fourier coefficient, T_0 is the period of the modulating function, and $f_0 = 1/T_0$ is the repetition frequency of the modulating function. If $f_c \gg f_0$ and all modulating functions share the same repetition frequency, then (2) can be substituted into (1) to express the TMAA array factor as:

$$AF(\theta) = \sum_{n=0}^{N-1} S_n e^{j\beta n d\sin\theta} \sum_{k=-\infty}^{+\infty} M_n[k] e^{j2\pi(f_c + f_0 k)t}. \tag{4}$$

Equation (4) shows that the time modulation generates spectral components at frequencies defined by $e^{j2\pi(f_c+f_0k)t}$ for $k \in \mathbb{Z}$. The amplitude of each spectral component depends on the angle θ; therefore, each can be considered a partial pattern of the TMAA. We can distinguish:

1) the central partial pattern ($k = 0$) related to the carrier frequency,
2) and the sideband partial patterns ($k \in \mathbb{Z},\ k \neq 0$) related to the frequencies located around the center frequency f_c at multiples of the time-modulation frequency f_0.

The central partial pattern is suitable for the suppression of sidelobes, whereas the sideband partial patterns can be used for a more flexible beamforming and beam-steering [22], [30]. Hereinafter, the terms *sideband* and *partial pattern* are used interchangeably.

B. Multi-Band Reception with the TMAA

Fig. 1 illustrates a receiving TMAA-based AAS in the presence of two transmitters. The adaptation goal is to maximize the power of the desired signal $s'(t)$ while suppressing the reception of the unwanted signal $s''(t)$. The carrier frequencies of the desired and unwanted signals are f'_c and f''_c, respectively, and $f'_c \neq f''_c$. To simplify the formulation we assume that $f''_c = f'_c + af_0$, where $a \in \mathbb{Z}$. Two array factors related to the desired (5) and unwanted (6) signals, respectively, can be formulated by analogy to (4). Both are composed of spectral components (i.e., sidebands) identified by indices k' and k'', respectively.

$$AF'(\theta) = \sum_{n=0}^{N-1} S'_n e^{j\beta' n d\sin\theta} \sum_{k'=-\infty}^{+\infty} M_n[k'] e^{j2\pi(f'_c + f_0 k')t} \tag{5}$$

$$AF''(\theta) = \sum_{n=0}^{N-1} S''_n e^{j\beta'' n d\sin\theta} \sum_{k''=-\infty}^{+\infty} M_n[k''] e^{j2\pi(f'_c + af_0 + f_0 k'')t} \tag{6}$$

An illustration of the frequency domain representation of the time-modulated desired and unwanted signals is presented in Fig. 2. To extract the components of AF' and AF'', which

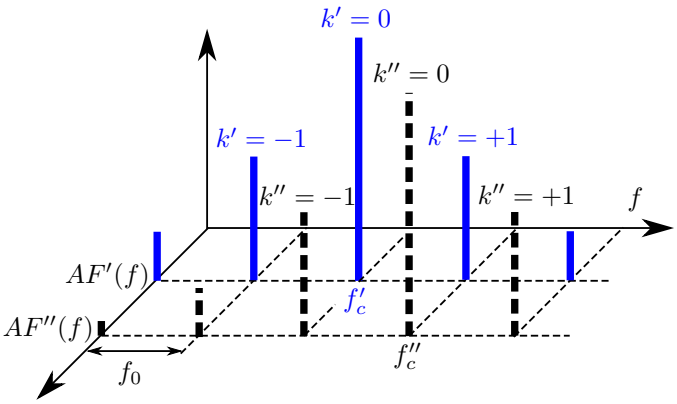

Fig. 2. Illustration of the time-modulated desired and unwanted signals in the frequency domain.

appear at the same frequency, we can compare the exponents as follows:

$$j2\pi(f_c' + f_0 k')t = j2\pi(f_c' + af_0 + f_0 k'')t, \tag{7}$$

which yields the relation between the indices of the spectral components that overlap:

$$k'' = k' - a. \tag{8}$$

Next, we can introduce variable f_x, which expresses the operational frequency of interest:

$$f_c' + f_0 k' = f_x. \tag{9}$$

The partial patterns over f_x can be obtained by substituting (8) and (9) into (5) and (6):

$$AF'(\theta, f_x) = e^{j2\pi f_x t} \sum_{n=0}^{N-1} S_n' e^{j\beta' nd \sin\theta} M_n[k'], \tag{10}$$

$$AF''(\theta, f_x) = e^{j2\pi f_x t} \sum_{n=0}^{N-1} S_n'' e^{j\beta'' nd \sin\theta} M_n[k' - a]. \tag{11}$$

The shapes of partial patterns (10) and (11) may diverge because they are formed by different sets of Fourier coefficients, i.e., $M_n[k']$ and $M_n[k' - a]$, respectively. The resultant array factor at frequency f_x is a superposition of (10) and (11):

$$AF'(\theta, f_x) + AF''(\theta, f_x) = e^{j2\pi f_x t} \sum_{n=0}^{N-1} \left(S_n' M_n[k'] + S_n'' M_n[k' - a]\right) e^{j\beta nd \sin\theta}, \tag{12}$$

where $\beta = \pi(f_c' + f_c'')/c = \pi(2f_c' + af_0)/c$ because if $f_c \gg f_0$, then $\beta' \approx \beta \approx \beta''$. Equation (12) demonstrates that the resultant signal at f_x is a combination of the desired and unwanted components and confirms that the reception of frequency-diverse signals with the TMAA can cause unwanted interference.

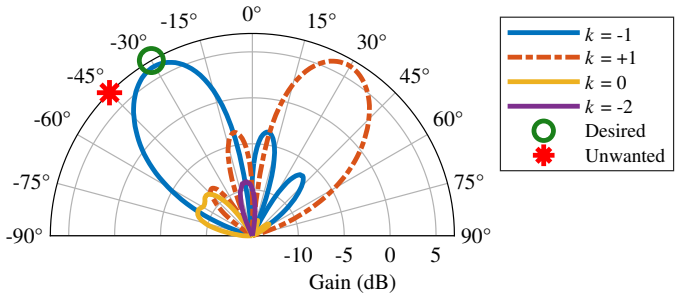

Fig. 3. Configuration of the TMAA showing four partial patterns, the direction of desired transmitter, and the direction of the unwanted transmitter.

TABLE I
CONFIGURATION OF THE TRANSMITTERS

	Desired	Unwanted
Modulation	Digital 16-QAM	Analog FM
Symbol rate	30 MS/s	N/A
Bit rate	120 Mb/s	N/A
Matched filter type	Root raised cosine	N/A
Roll-off factor	0.22	N/A
Signal bandwidth	36.6 MHz	30 MHz
Carrier frequency	5.6 GHz	5.55 GHz
Output power	5 dBm	0 dBm
Antenna type	Patch	Log-periodic
Antenna gain	6 dBi	8 dBi
Antenna HPBW	60°	80°
Direction	−30°	−45°

C. Case Study of Two Band-Pass Signals

To demonstrate the interference generated inherently by the TMAA from frequency-diverse band-pass signals, a practical use case was experimentally investigated as illustrated in Fig. 3. The experimental setup was composed of two transmitters (Table I) and the receiving TMAA arranged in the following manner:

1) The main beam of the partial pattern related to the first negative sideband ($k = -1$) was directed toward the desired transmitter ($\theta = -30°$), and the unwanted transmitter ($\theta = -45°$) was included within the half-power beam width (HPBW).
2) The central partial pattern related to the carrier frequency ($k = 0$) was suppressed.
3) The main beam of the partial pattern related to the first positive sideband ($k = +1$) was directed toward $\theta = +30°$.

Two frequency-diverse band-pass signals, i.e. the desired signal at the carrier frequency $f_c' = 5.6$ GHz and the unwanted signal at the carrier frequency $f_c'' = 5.55$ GHz, were impinging on the TMAA. Due to the time modulation with the frequency of 50 MHz the sidebands of these two signals were generated in the form of the spectral replicas at the frequencies listed in Table II. The spectral replicas of the desired and unwanted time-modulated signals are presented in Fig. 4. For instance, at $f_x = 5.55$ GHz, the first negative partial pattern ($k' = -1$) of the time-modulated desired signal overlapped the central partial pattern of the time-modulated unwanted signal ($k'' = 0$), causing an interference. The amplitudes of the desired and unwanted spectral replicas were

TABLE II
SIDEBANDS OF TWO SIGNALS GENERATED VIA TIME MODULATION

	k	Desired signal	Unwanted signal
Central component	0	5.60 GHz	5.55 GHz
1st positive sideband	+1	5.65 GHz	5.60 GHz
1st negative sideband	−1	5.55 GHz	5.50 GHz
2nd positive sideband	+2	5.70 GHz	5.65 GHz
2nd negative sideband	−2	5.50 GHz	5.45 GHz

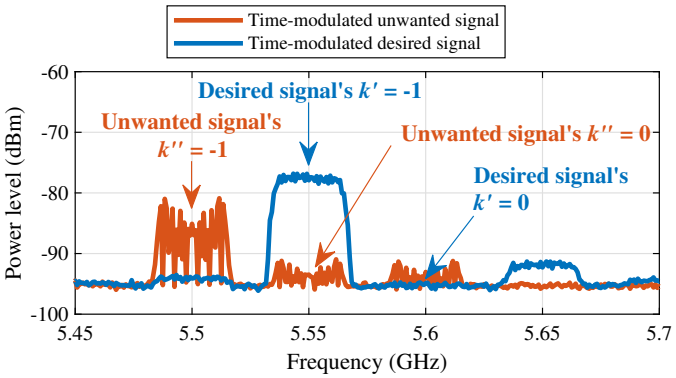

Fig. 4. Spectrum of the signals measured at the TMAA output for the configuration presented in Fig. 3 and signals specified in Table I.

different due to the different shapes of their related partial patterns. According to Fig. 3, the beam for $k' = -1$ was directed toward the signal source, explaining the high level of amplitude. Meanwhile, the partial pattern for $k'' = 0$ was substantially suppressed, however, it was not completely canceled. Therefore, at 5.55 GHz, the sideband of the desired signal dominated.

D. Design

The design of the TMAA used for the experimental adaptation study is presented in Fig. 1. The antenna array is composed of eight elements, each of which consists of two series-fed patch antennas. The return loss of each element is less than −10 dB in the frequency range of 5.4–5.8 GHz and the maximum gain is 9.8 dBi. The elements of the array are arranged oppositely and connected to radio-frequency (RF) switches, which are controlled by periodic rectangular signals with a repetition frequency of 50 MHz and adjustable delays Δt_n, where $n \in \{0, \ldots, 3\}$. Programmable digital delay lines (DDLs) with 8-bit registers are used to apply delay values from 0 to 15.3 ns, with a step of 60 ps. Therefore, 2^8 values per DDL are possible, yielding 2^{32} different configurations for a TMAA composed of four DDLs. A limited subset of all possible configurations provides practical results, e.g., beam-steering at sideband frequencies can be achieved when the delays progressively increase or decrease [31]. The TMAA demonstrates linear polarization, an HPBW of 24°, and a gain of 7 dBi, as measured at the first negative sideband. A detailed description of the design and principle of operation can be found in [32].

III. ADAPTIVE ALGORITHM

One of the primary motivations of this research was to design an algorithm that allows for real-time adaptation of

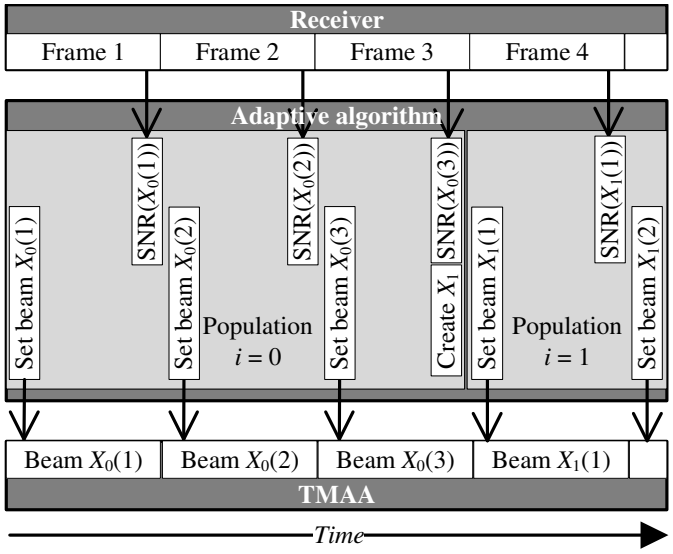

Fig. 5. Timing diagram of the AAS

a radiation pattern. The determination of an optimal radiation pattern was not anticipated because, in many practical applications, a significant improvement can be achieved even with a quasi-optimal solution. The operation of an algorithm is based on the quality indicator (QI) measured in the receiver. This approach is very reliable because it considers the various phenomena affecting a wireless transmission. In practice, the QI can be represented by many parameters, e.g., the SNR, the bit error rate, and the channel quality indicator (CQI). The duration between the steps of the proposed algorithm, i.e., its speed, depends primarily on the reporting interval, e.g., the minimum reporting interval of the CQI in the Long-Term Evolution cellular system is 1 ms [33]. For the purpose of this work a vector signal analyzer (VSA) was used to measure the SNR value every 200 ms.

The adaptation could be based on the GA, approach with binary-coded chromosomes representing the register values of the DDLs, which would lead to an extremely large search space (2^{32} configurations of the TMAA, of which many are impractical). However, better performance can be achieved with evolutionary programming (EP), in which the individuals evolve but do not exchange information among themselves and there are only mutation, not crossover, operators [34], [35]. In its basic form, EP is not suited for real-time adaptation because of a long convergence time. Therefore, the following modifications are proposed to the EP algorithm:

1) A limitation of the search space to 101 integer-coded individuals.
2) A limitation of the population size to three individuals.
3) A formulation of the fitness function based on the measurement data fetched from an operating receiver.

The individuals represent beams and are coded with integer numbers according to each respective direction. The search space is limited to 101 diverse beams directed from −50° to +50° with a step of 1°, which leads to a switched-beam adaptation. This increases the convergence rate, although its performance in the presence of interfering signals may be

moderate due to the absence of the null-forming capability.

A timing diagram, displaying the operation of the AAS during the first four data frames is presented in Fig. 5 (a data frame is considered as a certain amount of received samples for which the SNR is calculated in the receiving system). The individuals from the population are consecutively evaluated by applying a corresponding configuration to the TMAA. The SNR value is measured for each configuration and assigned as a fitness of each respective individual. For a given population $X_i = \{\chi_1, \chi_2, \ldots, \chi_l, \ldots \chi_L\}$, where i enumerates consecutive generations, $X_i(l) = \chi_l$ is the integer-coded individual, l is the index of the individual in the population, and L is the size of the population. The flowchart of the algorithm is presented in Fig. 6. It operates with the following steps:

- **Step 1: Initialization.** The initial population $X_0 = \{-30, 0, 30\}$ composed of $L = 3$ beams directed toward $-30°$, $0°$, and $+30°$ is defined. The diversely directed beams perform a coarse sense of the space in front of the TMAA.
- **Step 2: Fitness evaluation.** The beams are evaluated consecutively by a data frame. Each beam χ_l is set on the TMAA; then, a data frame is received, and the SNR is measured by a wireless system receiver. Next, the SNR is assigned as the fitness value of the corresponding individual. This step repeats L times for each beam in the population.
- **Step 3: Selection.** The beam for which the highest SNR is measured is considered to be closest to the direction of arrival (DoA); hence, it is selected as the top individual: $\chi_{\max} = \max_{X_i} \text{SNR}$. The maximum of the SNR achieved during the whole adaptation ($\text{SNR}_{\max}$) is updated.
- **Step 4: Reproduction.** A new population X_{i+1} (the offspring) is created based on the properties of the top individual $\chi_{\max}$. The offspring are composed of $L = 3$ individuals. The first one (χ_1) is an exact copy of $\chi_{\max}$, ensuring that the best beam from the last population is preserved. If the propagation conditions change, the top solution from the previous population might be obsolete. Therefore, two new beams (χ_2, χ_3) directed into a vicinity of $\chi_{\max}$ are added to the offspring. The directions of these two beams are provided by a customized mutation operator based on a random angular change $\xi_l = |r| \cdot \text{SNR}_{\text{drop}} \cdot c$, where r is a random variable from the normal distribution $\mathcal{N}(0, 1)$, $\text{SNR}_{\text{drop}} = \max(1, \text{SNR}_{\max} - \max\{\text{SNR}(X_i)\})$, and c is an empirical coefficient (herein $c = 4$). The angular change ξ_l is added to or subtracted from direction $\chi_{\max}$ to obtain two mutated individuals and, hence, two diverse beams: $\chi_2 = \chi_{\max} - \xi_2$ and $\chi_3 = \chi_{\max} + \xi_3$. The generation of mutated individuals is quasi-random; therefore, erroneous beams may occur. To avoid excessive beam diversity, the mutation range is controllable and depends on SNR_{drop}. If the beam $\chi_{\max}$ is directed toward the proximity of the DoA, then $\text{SNR}(\chi_{\max})$ is high, and the angular change ξ_l becomes small; hence, the beam directions in the next set will not significantly differ from $\chi_{\max}$. Conversely, if the DoA changes significantly and causes a substantial drop of $\text{SNR}(\chi_{\max})$, the new beams are quasi-randomly selected from a wider angular range to search for the DoA in more diverse directions. The offspring pass to Step 2 (the fitness evaluation), wherein the next three beams are consecutively applied to the TMAA.

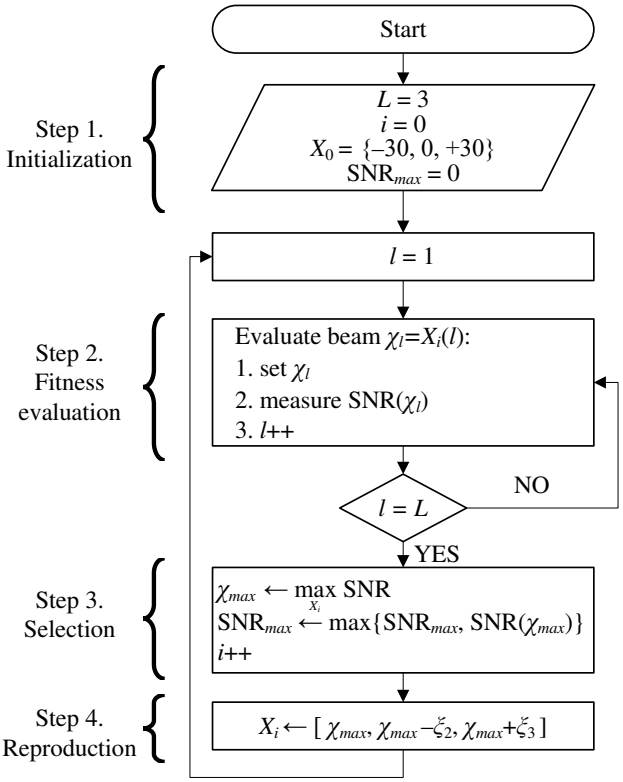

Fig. 6. Flowchart of the adaptive algorithm.

This procedure runs in a loop and corrects the quality of the wireless transmission in real-time.

IV. Experimental Evaluation of Adaptation in a Wireless Communication System

Fig. 7 presents the diagram of an experimental setup composed of the TMAA, a patch antenna, the log-periodic antenna R&S HL050, the signal generator (SG) R&S SMF100A, the vector signal generator (VSG) R&S SMBV100A, the spectrum analyzer (PSA) Agilent PSA E4440A, and a personal computer running the Keysight 89600 vector signal analyzer (VSA) software. The parameters of the desired transmitter (VSG) and unwanted transmitter (SG) are listed in Table I. The TMAA was used as a receiving antenna and was connected to the PSA input. Although the TMAA provides an infinite number of sidebands, to resemble the operation of a conventional single-channel receiver, the PSA was configured to acquire only the first negative sideband ($k = -1$) of the desired time-modulated signal (this particular sideband was selected due to a high gain and the beam-steering capability in a wide range of angles). The center frequency and frequency span of the PSA were set to 5.55 GHz and 36 MHz, respectively. The VSA software was used to demodulate the complex in-phase and quadrature

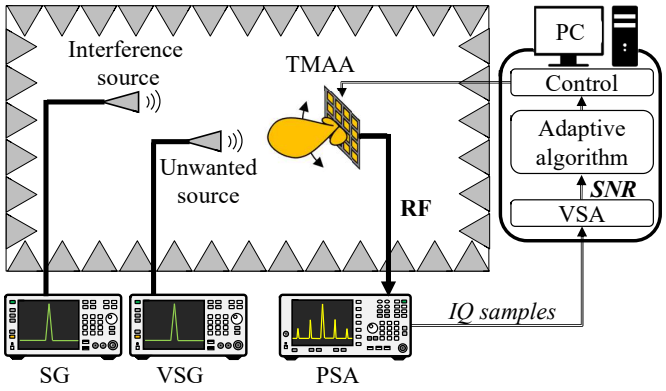

Fig. 7. Diagram of the experimental setup for the TMAA adaptation study.

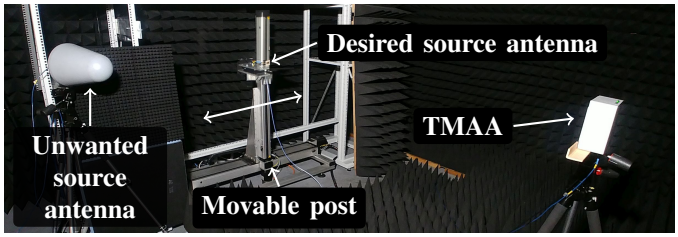

(a)

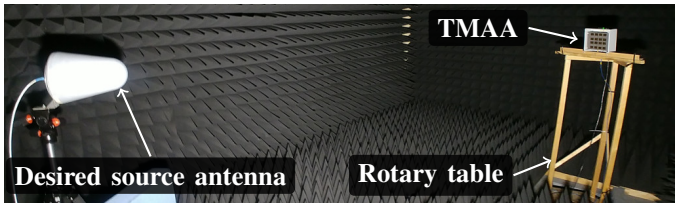

(b)

Fig. 8. Experimental setup for (a) two scenarios with gradual and linear motion and (b) one scenario with rapid and rotational motion.

(IQ) samples delivered from the PSA and calculate the SNR as the ratio of the average symbol power to the noise power according to the following equation:

$$\mathrm{SNR} = 10 \log \frac{\sum_{n=1}^{N} S_{\mathrm{ref}}^2}{\sum_{n=1}^{N} (S_{\mathrm{ref}} - S_{\mathrm{meas}})^2} \tag{13}$$

where N is the number of symbols in a single data frame, S_{ref} is the IQ reference symbol, and S_{meas} is the IQ measured symbol (the noise power includes anything that causes the symbol to deviate from the ideal state position, e.g., an additive noise, distortion, and interference) [36]. A successful demodulation required a minimum SNR of 15 dB; below this value, the synchronization algorithm of the VSA would fail. The experiments were conducted inside an anechoic chamber, as presented in Fig. 8. The mobility of the antennas was obtained with a movable post and a rotary table.

A. Scenario 1: Gradual Movement of the Mobile Terminal in an Isolated Environment

The primary purpose of the first scenario was to examine the performance of the adaptation when the location of a mobile terminal gradually changed, as illustrated in Fig. 9a. Due to the linear motion of the transmitting patch antenna, the DoA changed from $0°$ to $-30°$ and then back to $0°$, with an angular velocity of $2.5°$/s. The SNR was measured at each $0.5°$ increment of this change. The unwanted transmitter was then switched off.

Fig. 10a compares the actual values of the DoA and the direction of the TMAA beam set by the algorithm. A histogram of the accuracy (defined as the difference between

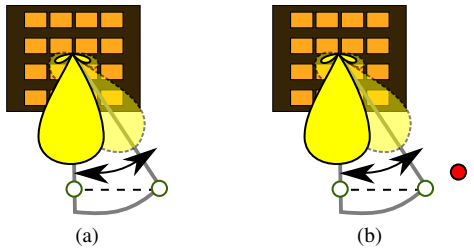

(a) (b)

Fig. 9. Illustration of the adaptation to the gradual movement of the desired source (a) in an isolated environment and (b) with an unwanted source (red dot).

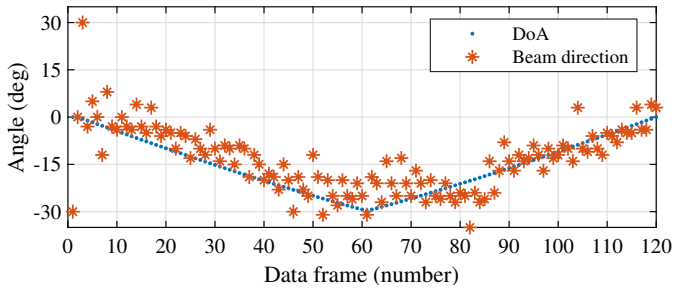

(a)

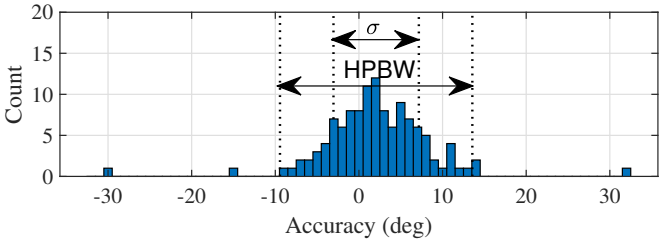

(b)

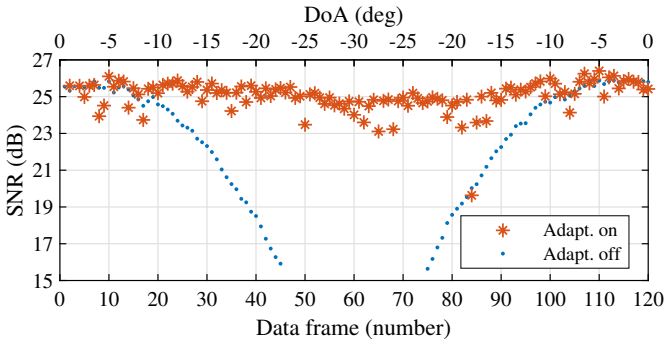

(c)

Fig. 10. Experimental scenario with a gradual change of the DoA. (a) Change of the DoA and adapted beam direction. (b) Change of the SNR during movement.

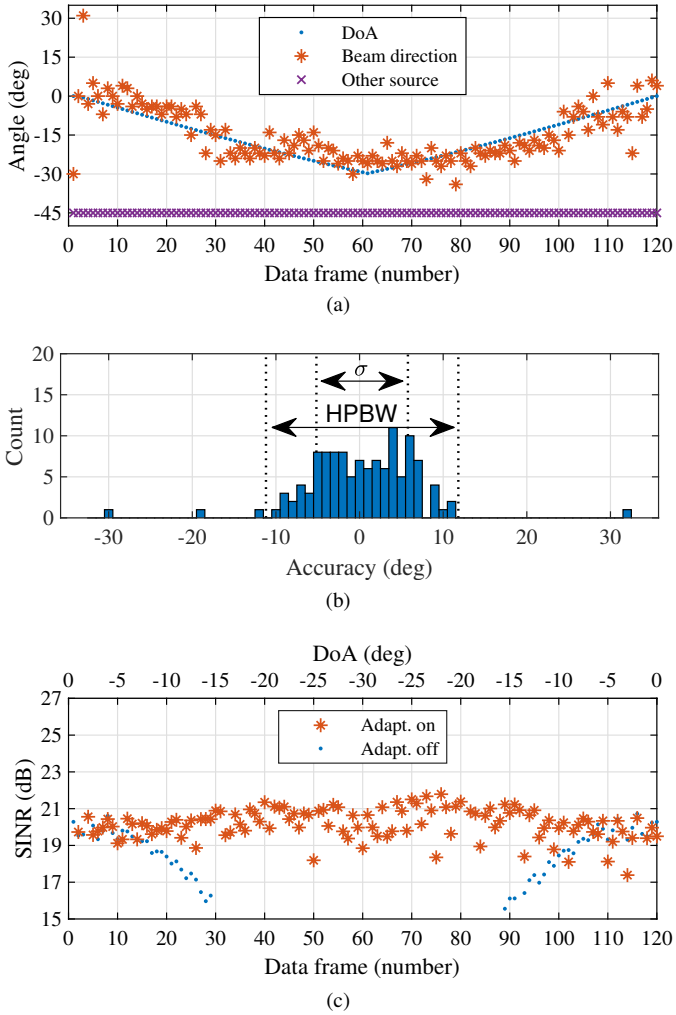

Fig. 11. Experimental scenario with multi-band reception. (a) Change of the DoA and adapted beam direction. (b) Change of the SINR during movement.

the beam's direction and the DoA) is presented in Fig. 10b. The histogram's distribution shows that the difference was converging to a mean value of 2°, although 0° was expected. The difference could be explained in that the beams selected for the next generation were based on the three previous measurements, which became obsolete due to the continuous movement of the patch antenna. The beams set by the algorithm matched the DoA with a maximum inaccuracy of ±10° (typically) and standard deviation (σ) of 5.1°. Both values were smaller than the HPBW of the TMAA. According to the measurements presented in Fig. 10c, the SNR was substantially improved compared with the case without adaptation, showing a very small variation for a wide range of tested angles and remaining above 15 dB, which is sufficient for a successful demodulation. Occasional drops were caused by the quasi-random characteristic of the algorithm.

B. Scenario 2: Gradual Movement of Mobile Terminal with Multi-Band Reception

In this scenario, as illustrated in Fig. 9b, the undesired source located at −45° was switched on. As a result, two band-pass signals (the desired signal at the carrier frequency

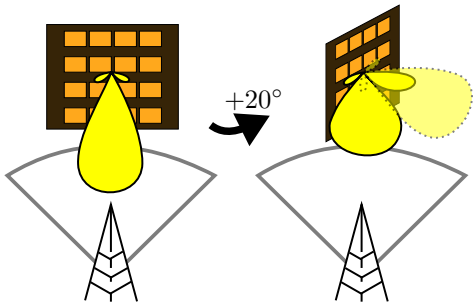

Fig. 12. Illustration of the adaptation to the rapid change of the DoA.

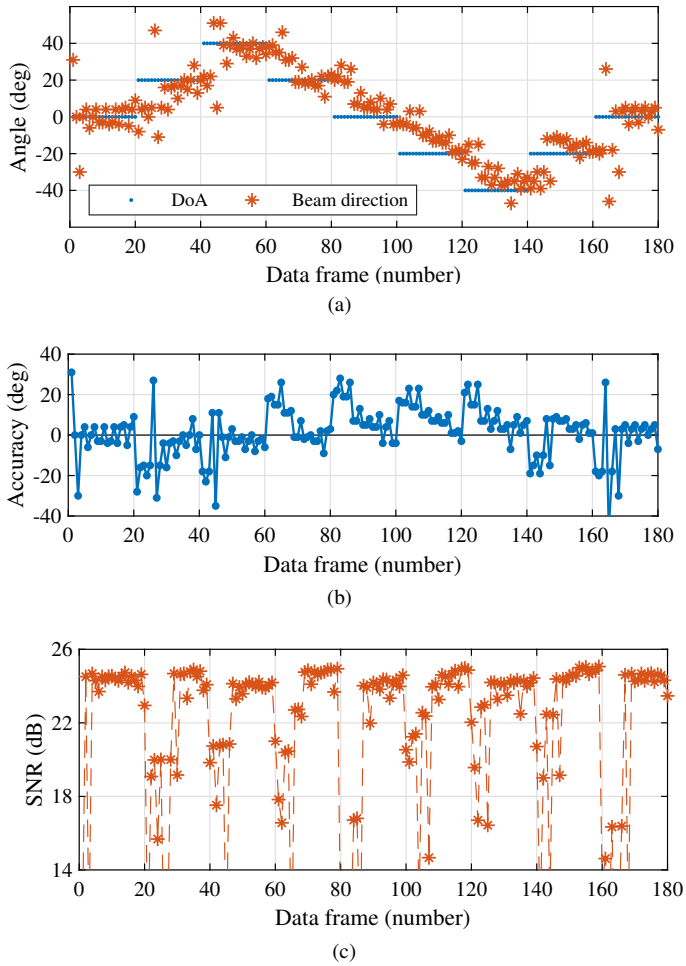

Fig. 13. Experimental scenario with rapid rotation. (a) Change of the DoA and adapted beam direction. (b) Change of the SNR during movement.

of 5.6 GHz and unwanted signal at the carrier frequency of 5.55 GHz) impinged on the TMAA. The sidebands generated from these two signals overlapped and created interference in the receiver, which affected the SNR. In this section, this is referred to as the signal-to-interference-plus-noise ratio (SINR). The direction of the beams selected by the adaptive algorithm are presented in Fig. 11a. The histogram presented in Fig. 11b more closely resembles a uniform distribution compared with Scenario 1 (without the unwanted signal), indicating a poorer performance of the minimization of the difference between the beam's direction and the DoA. However, this may not be a concern, because the antenna pattern with

a null pointed toward the direction of the unwanted source may have provided a higher SINR than the antenna pattern with the main beam ideally directed toward the DoA. Fig. 11c shows that stable values of the SINR were achieved even when the patch antenna was located close to the unwanted source (DoA $\approx -30°$).

C. Scenario 3: Rapid Angular Change

This scenario evaluated the performance of the adaptation when the orientation of the TMAA changes significantly and rapidly, as illustrated in Fig. 12. The TMAA was placed on a rotary table (Fig. 8b) to obtain a wider DoA range compared with the previous two scenarios. The unwanted transmitter was switched off and the desired transmitter was connected to the log-periodic antenna. The DoA changed with angular steps of 20° and remained stable for a duration of 20 data frames before the next change, as seen in Fig. 13a. Fig. 13b shows the difference between the beam's direction and the DoA. It typically converged to 0° after 10 data frames. Using an assumption of 200 ms per each SNR measurement, the adaptation to a substantial DoA change took approximately 2 s. As indicated by the measurements presented in Fig. 13c, as few as 5 data frames were sufficient to recover the SNR.

V. Conclusion

The reception of frequency-diverse signals via a TMAA may create interference in the receiving system. This peculiarity, which does not take place in conventional antenna systems, may be a significant disadvantage limiting the application of TMAAs in practical wireless networks. The beamforming properties of TMAAs provide an opportunity to mitigate this effect and improve a desired signal's strength by directing the main beam toward its arrival direction. The AAS proposed in this paper combines a wideband TMAA and an adaptive algorithm with a fitness evaluation based on the SNR measured in the receiver, providing real-time improvement of the SNR without complex computation. In this study, the obtained results demonstrated the feasibility of the TMAA adaptive beam-steering function and showed performance gains over a non-adaptive system.

References

[1] B. Widrow, P. E. Mantey, L. J. Griffiths, and B. B. Goode, "Adaptive antenna systems," *Proc. IEEE*, vol. 55, no. 12, pp. 2143–2159, Dec. 1967.

[2] I. Chiba, W. Chujo, and M. Fujise, "Beam space constant modulus algorithm adaptive array antennas," in *Proc. 8th Int. Conf. Antennas Propag.*, vol. 2, Edinburgh, UK, Mar. 1993, pp. 975–978.

[3] S. Choi and T. K. Sarkar, "Adaptive antenna array utilizing the conjugate gradient method for multipath mobile communication," *Signal Process.*, vol. 29, no. 3, pp. 319 – 333, Dec. 1992.

[4] D. H. Werner and R. Mittra, "Biological beamforming," in *Frontiers in Electromagnetics*. Wiley-IEEE Press, 2000.

[5] R. L. Haupt, "Phase-only adaptive nulling with a genetic algorithm," *IEEE Trans. Antennas Propag.*, vol. 45, no. 6, pp. 1009–1015, Jun. 1997.

[6] R. Haupt and H. Southall, "Experimental adaptive nulling with a genetic algorithm," *Microwave Journal*, vol. 42, no. 1, pp. 78–89, Jan. 1999.

[7] A. S. Hussaini, I. Elfergani, M. Abusitta, A. Adebola, R. Abd-Alhameed, T. Sadeghpour, M. Child, and J. Rodriguez, "Time modulated switching and reactive loading techniques applied to a circular array antenna using genetic algorithm optimisation," in *7th Eur. Conf. Antennas Propag. (EuCAP)*, Gothenburg, Sweden, Apr. 2013, pp. 347–351.

[8] Y. Yashchyshyn and M. Piasecki, "Improved model of smart antenna controlled by genetic algorithm," in *Proc. 6th Int. Conf. Experience of Designing and Applications of CAD Systems in Microelectronics (CADSM)*, Lviv–Slavsko, Ukraine, Feb. 2001, pp. 147–150.

[9] T. Su and H. Ling, "Array beamforming in the presence of a mounting tower using genetic algorithms," *IEEE Trans. Antennas Propag.*, vol. 53, no. 6, pp. 2011–2019, Jun. 2005.

[10] M. D. Migliore, D. Pinchera, and F. Schettino, "A simple and robust adaptive parasitic antenna," *IEEE Trans. Antennas Propag.*, vol. 53, no. 10, pp. 3262–3272, Oct. 2005.

[11] D. S. Weile and E. Michielssen, "The control of adaptive antenna arrays with genetic algorithms using dominance and diploidy," *IEEE Trans. Antennas Propag.*, vol. 49, no. 10, pp. 1424–1433, Oct. 2001.

[12] M. Donelli, R. Azaro, F. G. B. D. Natale, and A. Massa, "An innovative computational approach based on a particle swarm strategy for adaptive phased-arrays control," *IEEE Trans. Antennas Propag.*, vol. 54, no. 3, pp. 888–898, Mar. 2006.

[13] S. Yang, Y. B. Gan, and A. Qing, "Sideband suppression in time-modulated linear arrays by the differential evolution algorithm," *IEEE Antennas Wireless Propag. Lett.*, vol. 1, pp. 173–175, Feb. 2002.

[14] G. Li, S. Yang, Y. Chen, and Z.-P. Nie, "A novel electronic beam steering technique in time modulated antenna array," *Prog. Electromagn. Res.*, vol. 97, pp. 391–405, Jan. 2009.

[15] S. Yang, Y. B. Gan, and T. Peng Khiang, "A new technique for power–pattern synthesis in time–modulated linear arrays," *IEEE Antennas Wireless Propag. Lett.*, vol. 2, no. 1, pp. 285–287, 2003.

[16] P. Rocca, L. Poli, G. Oliveri, and A. Massa, "Adaptive nulling in time-varying scenarios through time-modulated linear arrays," *IEEE Antennas Wireless Propag. Lett.*, vol. 11, pp. 101–104, 2012.

[17] Y. Q. H. Li, Wen Tao and X. W. Shi, "Synthesis of conformal phased antenna arrays with a novel multiobjective invasive weed optimization algorithm," *Frequenz*, vol. 72, no. 5-6, pp. 209–219, Apr. 2017.

[18] J. Yang, W. T. Li, X. W. Shi, L. Xin, and J. F. Yu, "A hybrid ABC-DE algorithm and its application for time-modulated arrays pattern synthesis," *IEEE Trans. Antennas Propag.*, vol. 61, no. 11, pp. 5485–5495, Nov. 2013.

[19] S. Applebaum, "Adaptive arrays," *IEEE Trans. Antennas Propag.*, vol. 24, no. 5, pp. 585–598, Sep. 1976.

[20] Y. Yashchyshyn, J. Marczewski, K. Derzakowski, J. W. Modelski, and P. B. Grabiec, "Development and investigation of an antenna system with reconfigurable aperture," *IEEE Trans. Antennas Propag.*, vol. 57, no. 1, pp. 2–8, Mar. 2009.

[21] J. D. Fredrick, Y. Wang, and T. Itoh, "A smart antenna receiver array using a single RF channel and digital beamforming," *IEEE Trans. Microw. Theory Techn.*, vol. 50, no. 12, pp. 3052–3058, Dec. 2002.

[22] R. Maneiro-Catoira, J. Brégains, J. A. García-Naya, and L. Castedo, "Time modulated arrays: from their origin to their utilization in wireless communication systems," *Sensors*, vol. 17, no. 3, p. 590, Mar. 2017.

[23] W. Kummer, A. Villeneuve, T. Fong, and F. Terrio, "Ultra-low sidelobes from time-modulated arrays," *IEEE Trans. Antennas Propag.*, vol. 11, no. 6, pp. 633–639, Dec. 1963.

[24] R. Maneiro-Catoira, J. C. Brégains, J. A. García-Naya, and L. Castedo, "On the feasibility of time-modulated arrays for digital linear modulations: A theoretical analysis," *IEEE Trans. Antennas Propag.*, vol. 62, no. 12, pp. 6114–6122, Dec. 2014.

[25] G. Bogdan and Y. Yashchyshyn, "Experimental study of signal reception by means of time-modulated antenna array," in *21st Int. Conf. Microw. Radar Wireless Commun. (MIKON)*, Kraków, Poland, May 2016, pp. 1–4.

[26] D. Masotti, A. Costanzo, M. D. Prete, and V. Rizzoli, "Time-modulation of linear arrays for real-time reconfigurable wireless power transmission," *IEEE Trans. Microw. Theory Techn.*, vol. 64, no. 2, pp. 331–342, Feb. 2016.

[27] A.-M. Yao, W. Wu, and D.-G. Fang, "Single-sideband time-modulated phased array," *IEEE Trans. Antennas Propag.*, vol. 63, no. 5, pp. 1957–1968, May 2015.

[28] R. Maneiro-Catoira, J. Brégains, J. A. García-Naya, and L. Castedo, "Time-modulated phased array controlled with nonideal bipolar squared periodic sequences," *IEEE Antennas Wireless Propag. Lett.*, vol. 18, no. 2, pp. 407–411, 2019.

[29] R. Maneiro-Catoira, M. Bernice Angoue Avele, J. Brégains, J. A. García-Naya, and L. Castedo, "Beam-steering in switched 4D arrays based on the discrete Walsh transform," in *27th Eur. Signal Processing Conf. (EUSIPCO)*, A Coruña, Spain, Sep. 2019, pp. 1–5.

[30] L. Poli, P. Rocca, G. Oliveri, and A. Massa, "Harmonic beamforming in time-modulated linear arrays," *IEEE Trans. Antennas Propag.*, vol. 59, no. 7, pp. 2538–2545, Jul. 2011.

[31] G. Bogdan, P. Bajurko, and Y. Yashchyshyn, "Null-steering in two-element time modulated linear antenna array through pulse-delay approach," in *20th Int. Conf. Microw. Radar Wireless Commun. (MIKON)*, Gdańsk, Poland, Jun. 2014, pp. 1–4.
[32] G. Bogdan, K. Godziszewski, Y. Yashchyshyn, C. H. Kim, and S. Hyun, "Time modulated antenna array for real-time adaptation in wideband wireless systems—Part I: Design and characterization," *IEEE Trans. Antennas Propag.*, 2019. [Online]. Available: https://ieeexplore.ieee.org/document/8657780
[33] 3GPP, *TS 36.213: Evolved Universal Terrestrial Radio Access (E-UTRA); Physical layer procedures*, Std., 2018.
[34] A. Hoorfar, "Evolutionary programming in electromagnetic optimization: A review," *IEEE Trans. Antennas Propag.*, vol. 55, pp. 523–537, Mar. 2007.
[35] S. K. Goudos, C. Kalialakis, and R. Mittra, "Evolutionary algorithms applied to antennas and propagation: A review of state of the art," *Int. J. Antennas Propag.*, vol. 2016, pp. 1–12, 2016.
[36] Keysight Technologies, *89600 VSA Software Help Documentation*, 2019.

Grzegorz Bogdan (S'16–M'19) was born in Poland in 1989. He received his M.E. and Ph.D. degrees in telecommunications from the Warsaw University of Technology (WUT), Warsaw, Poland in 2013 and 2019, respectively. Since 2019 he is an Assistant Professor at WUT in the Institute of Radioelectronics and Multimedia Technology of the Faculty of Electronics and Information Technology. His main research interests are design and optimization of adaptive antenna arrays and wireless communication systems.

Konrad Godziszewski (S'12–M'17) was born in Warsaw, Poland, in 1986. He received the M.E. degree in electronics and telecommunications in 2011, and the Ph.D. in telecommunications in 2018, both from Warsaw University of Technology (WUT), Warsaw, Poland. He joined the Institute of Radioelectronics and Multimedia Technology, WUT, in 2013 where he is currently an Assistant Professor. He has authored or coauthored over 50 technical papers. His current research interests include antennas, material characterization in sub-terahertz frequency range, and ferroelectric materials.

Yevhen Yashchyshyn (M'96–SM'09) received the M.E. degree from Lviv Polytechnic National University, Lviv, Ukraine, in 1979, the Ph.D. degree from Moscow Institute of Electronics and Mathematics (MIEM), Moscow, Russia, in 1986, and the D.Sc. (Habilitation) degree from Warsaw University of Technology (WUT), Warsaw, Poland, in 2006. In 2016 he was promoted to a Professor Title. Since 1999 he has been with the Institute of Radioelectronics and Multimedia Technology, WUT. He has authored over 250 technical papers, authored or coauthored 5 books, and holds a few patents. His current research interests include antenna theory and techniques, smart beamforming, reconfigurable antennas, radio over fiber techniques, and materials characterization, including ferroelectric ceramic-polymers composites investigation up to subterahertz frequency. Prof. Yashchyshyn was the recipient of the First Prize of EuMA at the 11th European Microwave Week for his outstanding research and new concept of the reconfigurable antenna, Amsterdam, the Netherlands, 2008.